CrossMark

Binary copper and iron oxides immobilized on silica-layered magnetite as a new reusable heterogeneous nanostructure catalyst for the Knoevenagel condensation in water

Masumeh Gilanizadeh[1] · Behzad Zeynizadeh[1]

Abstract In this study, a novel heterogeneous and reusable nanostructure catalyst was synthesized through the immobilization of bimetallic Cu–Fe mixed oxides on silica-layered magnetite. The prepared nanomagnetic $Fe_3O_4@SiO_2@CuO–Fe_2O_3$ was characterized using Fourier-transform infrared spectroscopy, scanning electron microscopy, energy-dispersive X-ray spectroscopy (EDX), X-ray diffraction, Brunauer–Emmett–Teller analysis, thermogravimetric analysis, differential thermal gravity, a vibration sample magnetometer, transmission electron microscopy and inductively coupled plasma optical emission spectroscopy. The catalytic activity of this mesoporous nanocomposite was studied in the Knoevenagel condensation of aromatic aldehydes and malononitrile in water to afford benzylidenemalononitriles in high to excellent yields. The nanocatalyst was able to be recycled five times without a significant loss in catalytic activity. This nanostructure catalyst allows for mild reaction conditions and acceptable reaction times, while delivering the desired products in high purity and yield without the use of dangerous organic solvents.

Keywords Benzylidenemalononitriles · $Fe_3O_4@SiO_2@CuO–Fe_2O_3$ · Knoevenagel condensation · Malononitrile · Nanocatalyst

---

✉ Masumeh Gilanizadeh
masumehgilanizadeh@gmail.com

1 Faculty of Chemistry, Urmia University, Urmia 5756151818, Iran

Introduction

Heterogeneous catalysis is utilized extensively today for facilitating a wide variety of organic reactions in both academic and industrial settings [1–12]. Numerous papers and documents show the importance of this type of catalysis [13–21]. Among the many heterogeneous catalysts, metal oxides exhibit a high level of activity, and they can be readily used as either active phases or solid supports for the immobilization of other promoters [22]. In this context, metal oxides containing transition metals are the subject of increasing interest because of their inexpensive preparation, ease of regeneration and selectivity. These materials are generally classified by their crystalline systems and they are prepared in the form of a powder or as single crystals. In addition, they are widely used in electronics, nuclear research and ceramics [23–25].

Mixed metal oxides have two or more types of metal cations. According to the number of diverse metal cations, they can be categorized as binary, ternary and quaternary oxides. Hydrothermal methods [26, 27], mechanochemical synthesis [28, 29], sol–gel [30–33], co-precipitation [34, 35], wet impregnation [36, 37] and microwave irradiation [38] are commonly used for the preparation of mixed metal oxides.

Recently, systems combining magnetic nanoparticles (MNPs) and mixed metal oxides have been developed for application in numerous processes, due to the vast surface area of the nanoparticles as well as the presence of acidic/basic sites on the metal oxides which improve the promoter activity and selectivity of the mixed composite systems. Moreover, they are easily separated by an external magnetic field at the end of reaction [39–49]. In this context, a number of manuscripts highlight the usefulness of mixed metal oxides as catalysts in several synthetic transformations [50–58].

The Knoevenagel condensation is an important reaction used to install C=C bonds in organic compounds. The reaction occurs via nucleophilic attack of an active methylene group to an aldehyde followed by dehydration [59]. This method is suitable for the preparation of structurally diverse alkene compounds which can be utilized as intermediates for numerous reactions [60]. Generally, benzylidene-malononitriles (BMNs) are synthesized by the Knoevenagel condensation of aromatic aldehydes and malononitrile. BMN derivatives have been widely used in biological and pharmaceutical studies. They exhibit various properties including anti-inflammatory, anticonvulsant, antioxidant and anticancer activity [61, 62]. Several useful procedures have been reported for synthesis of BMN derivatives [63–80]. Although most of the reported methods have their own merits, however, they generally suffer from disadvantages such as the use of expensive organic solvents or catalysts, harsh reaction conditions, prolonged reaction times, undesirable yields and tedious work-up procedures. Therefore, further efforts are needed towards the development and introduction of easy protocols which use effective catalysts under mild and green reaction conditions is still demanded.

In this study, we wish to introduce $Fe_3O_4@SiO_2@CuO–Fe_2O_3$, a new type of magnetic mixed metal oxide that can be successfully utilized for the Knoevenagel

condensation of diverse aromatic aldehydes with malononitrile to afford benzylidenemalononitrile products in high to excellent yields. All reactions were carried out in refluxing H_2O (Scheme 1).

Results and discussion

Synthesis and characterizations of the nanocatalyst

Magnetic nanoparticles of $Fe_3O_4@SiO_2@CuO–Fe_2O_3$ were synthesized through a three-step procedure: (1) the preparation of magnetite nanoparticles by a chemical co-precipitation of $FeCl_2·4H_2O$ and $FeCl_3·6H_2O$ in an aqueous solution of ammonia, (2) coating of SiO_2 on the surface of magnetite-cores by tetraethyl orthosilicate (TEOS) at room temperature, and (3) the use of an in situ growth method to immobilize Cu^{2+} and Fe^{3+} salts on the core of silica-layered magnetite followed by calcinations at 150 °C to prepare magnetic nanoparticles of $Fe_3O_4@SiO_2@CuO–Fe_2O_3$ MNPs (Scheme 2).

Nanocatalyst characterization

Fourier-transform infrared spectroscopy (FTIR)

FTIR spectroscopy is a useful technique for the structural elucidation of compounds. In this context, the FTIR spectrum of nano Fe_3O_4 (Fig. 1a) exhibits a strong absorption peak at 575 cm^{-1} corresponding to vibration of Fe–O bonds. The absorption peaks at 3400 and 1625 cm^{-1} are attributed to O–H stretching and deforming vibrations of adsorbed water, respectively. FTIR spectrum of $Fe_3O_4@SiO_2$ MNPs is also illustrated in Fig. 1b. The spectrum shows additional peaks at 796 and 1094 cm^{-1} that are assigned to the symmetrical and asymmetrical Si–O–Si stretching vibrations. These results confirm the successful layering of SiO_2 on the cores–surface of magnetite. The FTIR spectrum of $Fe_3O_4@SiO_2@CuO–Fe_2O_3$ MNPs (Fig. 1c) exhibits a wide and strong absorption band around 3200–3600 cm^{-1} that corresponds to superimposed hydroxyl stretching bands arising from the O–H bond of water within the layers. An additional absorption band around 1600 cm^{-1} can be attributed to the deforming mode of water molecules. In addition, the absorption peaks around 400–600 cm^{-1} are attributed to the vibration modes of Fe–O and Cu–O bonds, which confirms the formation of mixed $CuO–Fe_2O_3$ on the cores–surface of $Fe_3O_4@SiO_2$.

R = H, Me, OMe, NO_2, OH, Cl, CHO
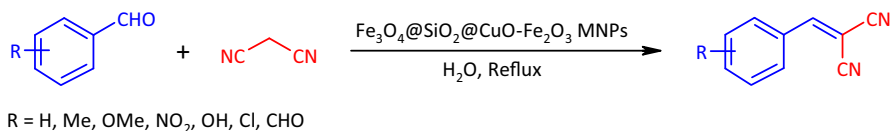
Scheme 1 Synthesis of benzylidenemalononitriles by $Fe_3O_4@SiO_2@CuO–Fe_2O_3$ MNPs
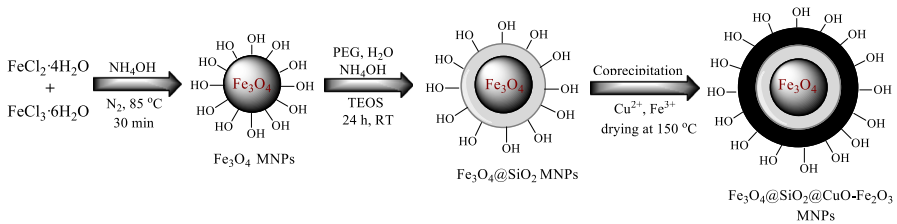
Scheme 2 Synthesis of $Fe_3O_4@SiO_2@CuO–Fe_2O_3$ MNPs

Fig. 1 FTIR spectrum of
a Fe_3O_4, **b** $Fe_3O_4@SiO_2$ and
c $Fe_3O_4@SiO_2@CuO–Fe_2O_3$
MNPs
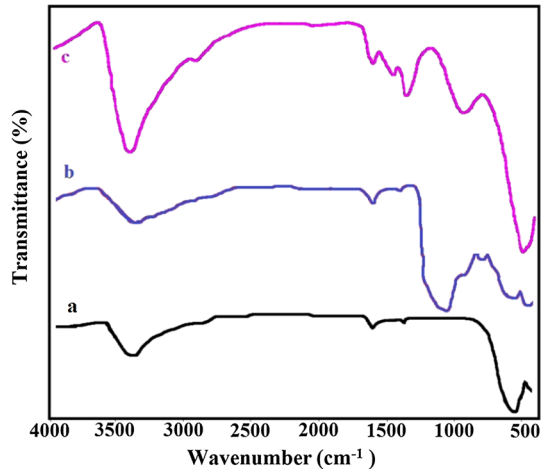
Scanning electron microscopy (SEM)

SEM is commonly used to determine the size distribution and morphology of the synthesized particles. SEM images of Fe_3O_4, $Fe_3O_4@SiO_2$ and $Fe_3O_4@SiO_2@CuO–Fe_2O_3$ MNPs are illustrated in Fig. 2. The images indicate that the immobilized $CuO–Fe_2O_3$ on silica-layered magnetite was constructed from roughly spherical and granule particles. In addition, particles of Fe_3O_4, $Fe_3O_4@SiO_2$ and $Fe_3O_4@SiO_2@CuO–Fe_2O_3$ MNPs are distributed in the range of 23–43 nm (Fig. 2a), 22–30 nm (Fig. 2b) and 27–29 nm (Fig. 2c–f), respectively. The meso-porous structure of $Fe_3O_4@SiO_2@CuO–Fe_2O_3$ MNPs is determined based on the size of the nanoparticles.

Energy-dispersive X-ray spectroscopy (EDX)

The elemental composition of a material can be determined by electron dispersive X-ray spectroscopy (EDX–SEM). Figure 3 shows the elemental analysis and EDX spectrum of $Fe_3O_4@SiO_2@CuO–Fe_2O_3$ MNPs. The analysis shows that Fe, Cu, Si and O are present in the nanocomposite. Therefore, the copper–iron oxide layer was successfully coated on the cores–surface of $Fe_3O_4@SiO_2$ MNPs.
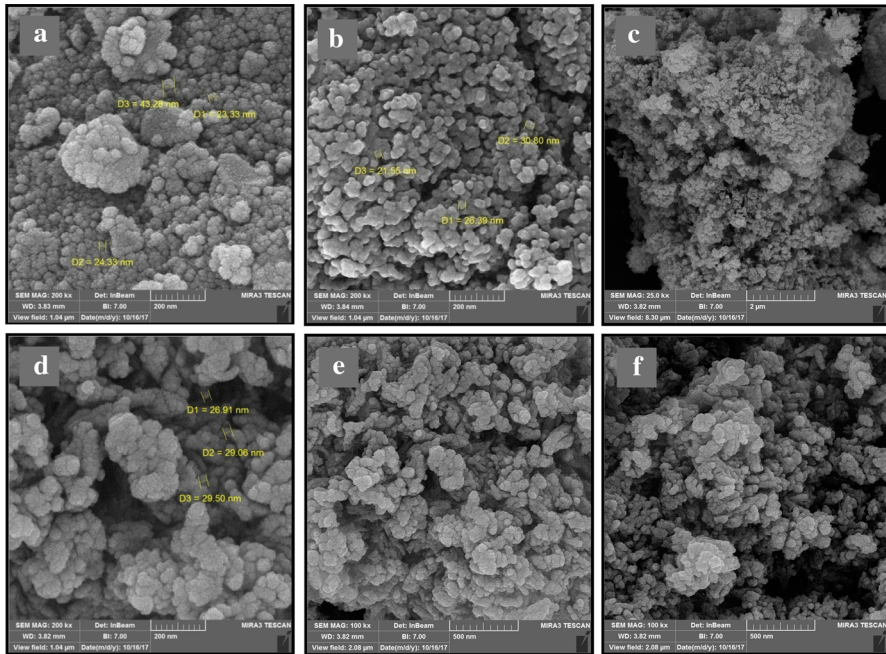
Fig. 2 FE-SEM image of **a** Fe_3O_4, **b** $Fe_3O_4@SiO_2$ and **c–f** $Fe_3O_4@SiO_2@CuO–Fe_2O_3$ MNPs
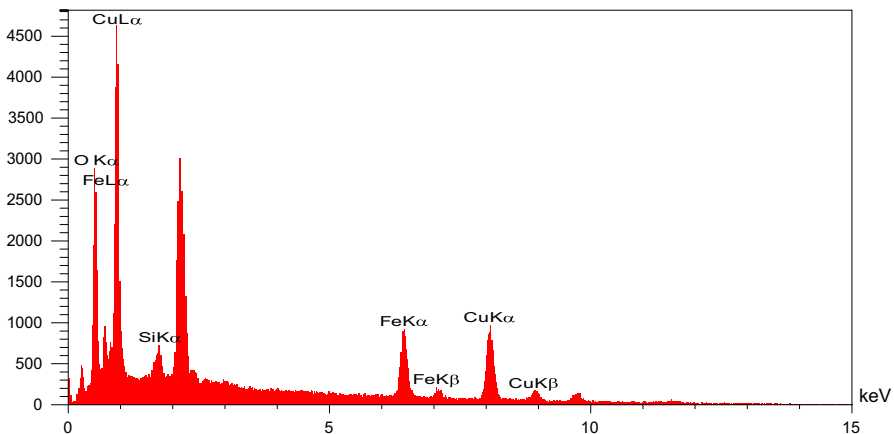
Fig. 3 EDX spectrum of $Fe_3O_4@SiO_2@CuO–Fe_2O_3$ MNPs

X-ray diffraction (XRD)

The crystalline structure of Fe_3O_4, $Fe_3O_4@SiO_2$ and $Fe_3O_4@SiO_2@CuO–Fe_2O_3$ MNPs was also analyzed by X-ray diffraction (XRD). Figure 4a shows the diffraction peaks at $2\theta = 30.2°$, $35.5°$, $43.3°$, $53.7°$, $57.2°$ and $62.9°$ corresponding to (220), (311), (400), (422), (511) and (440) crystal planes of nano Fe_3O_4. Based on

Fig. 4 XRD pattern of **a** Fe$_3$O$_4$,
b Fe$_3$O$_4$@SiO$_2$ and
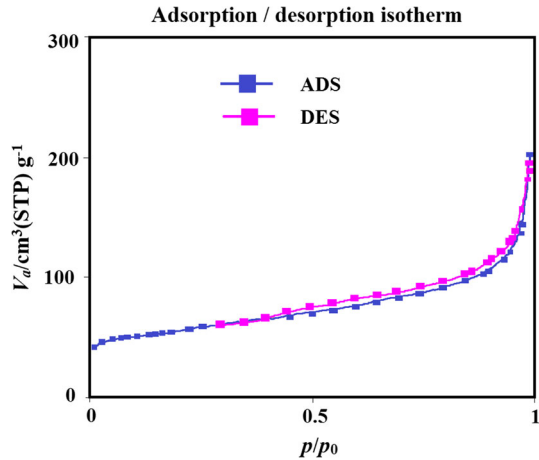**c** Fe$_3$O$_4$@SiO$_2$@CuO–Fe$_2$O$_3$
MNPs
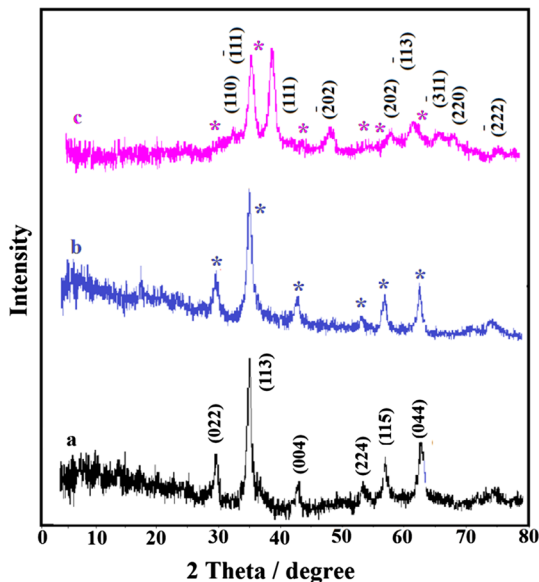
this pattern, the prepared laboratory sample of magnetite has a crystalline cubic spinel structure analogous to the standard structure of Fe$_3$O$_4$ (JCPDS 65-3107) [81, 82]. The XRD pattern of Fe$_3$O$_4$@SiO$_2$ MNPs is illustrated in Fig. 4b. Analysis of this spectrum shows that the pattern is identical to that of Fe$_3$O$_4$, while the intensity of the peaks decreased to some extent. This is attributed to crystalline phase-intact of Fe$_3$O$_4$ through layering of SiO$_2$ on the cores of Fe$_3$O$_4$. In the XRD pattern of Fe$_3$O$_4$@SiO$_2$@CuO–Fe$_2$O$_3$ MNPs, all characteristic peaks of Fe$_3$O$_4$ are also observable. Furthermore, the peaks at 2θ = 32.5°, 35.5°, 38.7°, 48.7°, 58.3°, 61.5°, 66.2°, 68.1° and 75.2° corresponded to (110), (-111), (111), (-202), (202), (-113), (-311), (220) and (-222) crystal planes, which proves the monoclinic crystalline structure of Fe$_3$O$_4$@SiO$_2$@CuO–Fe$_2$O$_3$ MNPs. It is in agreement with the documented-crystalline structure of copper oxide in JCPDS 80-1916 [83]. Through the Debye–Scherrer equation ($D = k\lambda/\beta\cos\theta$), the mean particle size of Fe$_3$O$_4$@SiO$_2$@CuO–Fe$_2$O$_3$ MNPs was calculated to be 9.67 nm. In this equation, β is the full width at half maximum intensity (FWHM) and is equal to 0.91° (0.016 rad) at θ = 19.50°.

Brunauer–Emmett–Teller (BET)

The nitrogen adsorption and desorption isotherms of the synthesized Fe$_3$O$_4$@SiO$_2$@CuO–Fe$_2$O$_3$ MNPs is illustrated in Fig. 5. The surface area and pore size distribution of the nanocatalysts were examined by BET and BJH methods. The calculated BET specific surface area (S_{BET}) is 128.03 m^2 g^{-1} and the pore volume (V_p) is 0.279 cm^3 g^{-1}. The obtained results suggest a high specific surface area to volume ratio for the nanocatalyst, leading to a dramatic increase in its catalytic activity. Through the Barrett–Joyner–Halenda (BJH) method, the

average pore size of the nanocomposite was determined to be 8.716 nm, confirming the mesoporous structure of $Fe_3O_4@SiO_2@CuO–Fe_2O_3$ MNPs.

Thermogravimetric analysis (TGA)

The thermal behavior, possible thermal stability and degradation processes of the synthesized MNPs were examined by thermogravimetric analysis (TGA). The located contents on the surface of MNPs can be generally determined by TGA analysis. Figure 6a shows TGA-thermograph of Fe_3O_4, which demonstrates the high thermal stability of magnetite at elevated temperature. Figures 6b and 7a represent TGA and DTG thermographs of $Fe_3O_4@SiO_2$ MNPs with two thermal degradation steps. The 2.18% loss of mass in the range of 30–158 °C (first decomposition step)

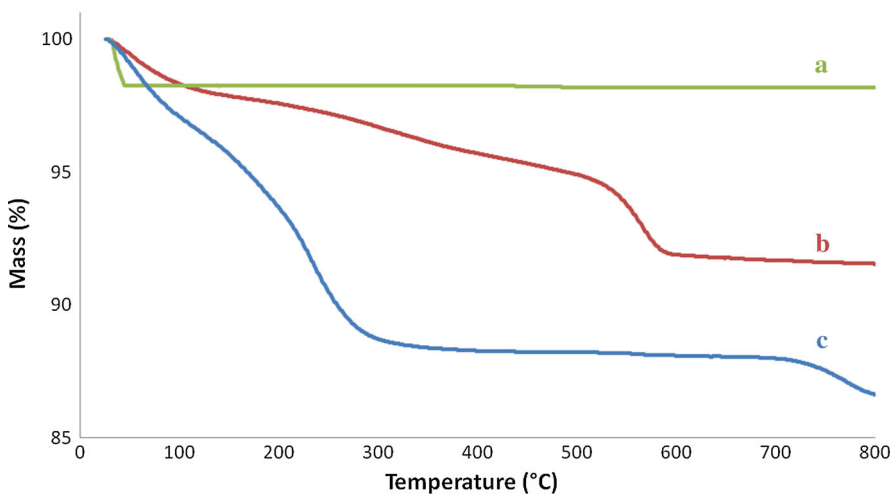**Fig. 6** TGA thermogram of **a** Fe_3O_4, **b** $Fe_3O_4@SiO_2$ and **c** $Fe_3O_4@SiO_2@CuO–Fe_2O_3$ MNPs
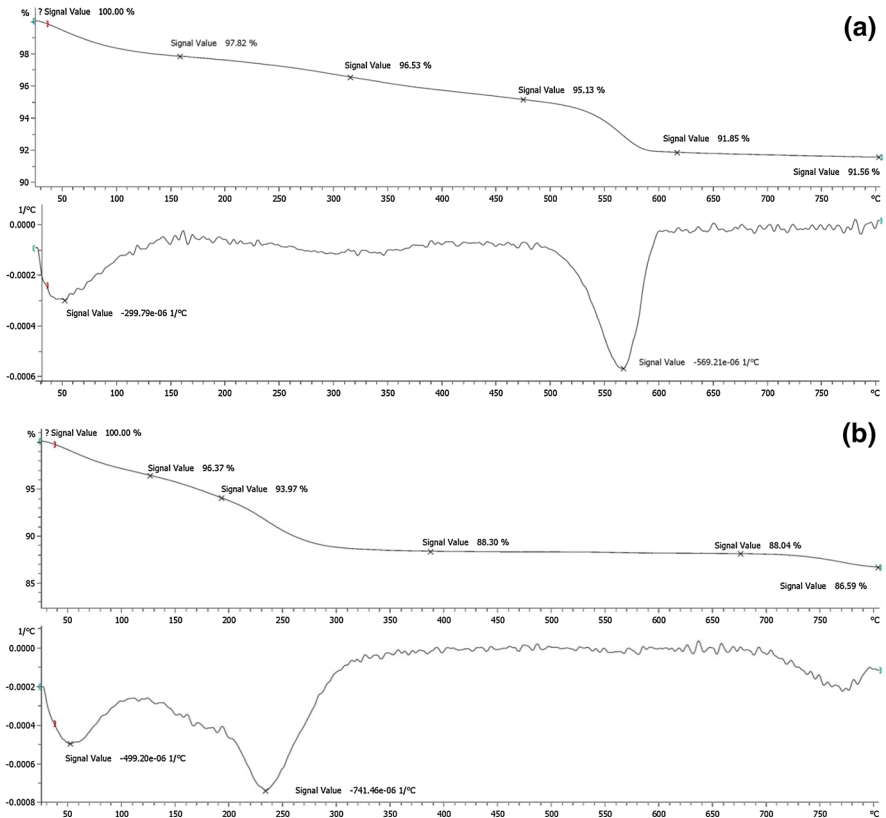
Fig. 7 TGA and DTG of **a** $Fe_3O_4@SiO_2$ and **b** $Fe_3O_4@SiO_2@CuO–Fe_2O_3$ MNPs

corresponds to the evaporation of adsorbed solvent or water. The second degradation step (loss of 3.28% mass) is observed at 474–616 °C and it is attributed to the degradation of the SiO_2 layer. Figures 6c and 7b illustrate TGA and DTG thermographs of $Fe_3O_4@SiO_2@CuO–Fe_2O_3$ MNPs with two thermal degradation steps. The first loss of mass is identified in the range of 26–127 °C (loss of 3.62% mass) and is attributed to the elimination of adsorbed water at the surface. The second loss of mass in the range of 193–384 °C (loss of 5.66% mass) corresponds to the degradation of the $CuO–Fe_2O_3$ or SiO_2 layers.

Vibration sample magnetometer (VSM)

Magnetic characterization of the prepared nanoparticles by vibrating sample magnetometer analysis is illustrated in Fig. 8. The curves represent the super paramagnetic behavior of MNPs appearing in reversible and nonlinear platforms. The saturation magnetization (Ms) values of Fe_3O_4 (Fig. 8a), $Fe_3O_4@SiO_2$ (Fig. 8b) and $Fe_3O_4@SiO_2@CuO–Fe_2O_3$ (Fig. 8c) MNPs were found to be 70, 30 and 4 emu g^{-1}, respectively. The graphs depict a decrease in the saturation

Fig. 8 Hysteresis loop of
a Fe$_3$O$_4$, **b** Fe$_3$O$_4$@SiO$_2$ and
c Fe$_3$O$_4$@SiO$_2$@CuO–Fe$_2$O$_3$
MNPs
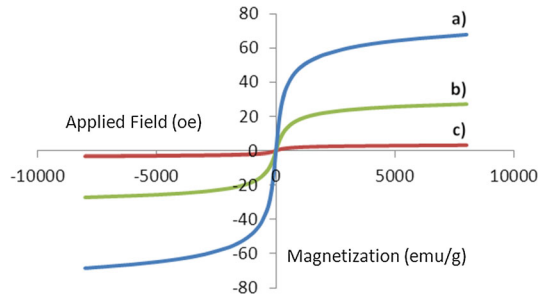
magnetization (Ms) of Fe$_3$O$_4$-cores caused by encapsulation with SiO$_2$ or CuO–Fe$_2$O$_3$ layers.

Transmission electron microscopy (TEM)

The obtained transmission electron microscope (TEM) images of Fe$_3$O$_4$@SiO$_2$@CuO–Fe$_2$O$_3$ MNPs (Fig. 9) show that the nanocatalyst has the core–shell nanostructure platform.

Inductively coupled plasma optical emission spectroscopy (ICP-OES)

The ICP-OES technique is generally utilized to determine the exact elemental composition of a compound. Through this analysis, the quantities of Fe and Cu in Fe$_3$O$_4$@SiO$_2$@CuO–Fe$_2$O$_3$ MNPs were determined to be 28.38, and 45.61%, respectively.
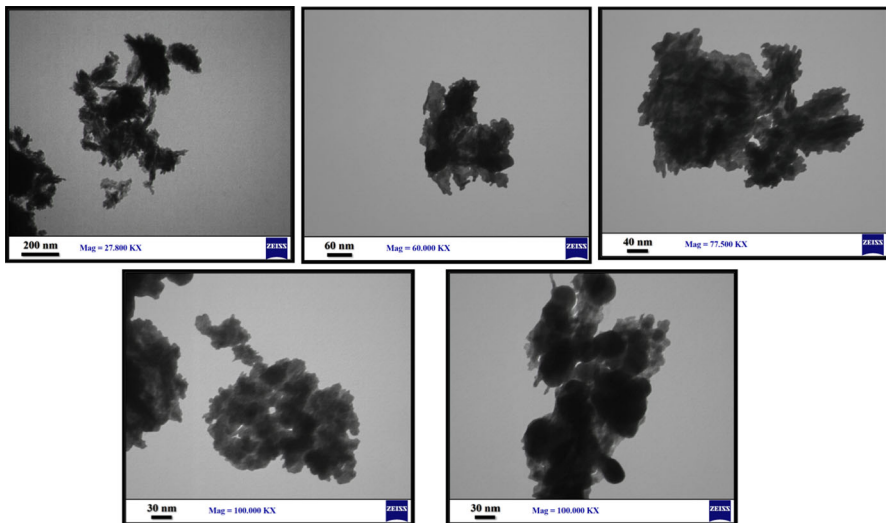
Fig. 9 TEM images of Fe$_3$O$_4$@SiO$_2$@CuO–Fe$_2$O$_3$ MNPs

Synthesis of benzylidenemalononitrile derivatives

After the successful synthesis of $Fe_3O_4@SiO_2@CuO–Fe_2O_3$ MNPs, the catalytic activity of the heterogeneous nanocatalyst towards the Knoevenagel condensation of aromatic aldehydes with malononitrile in H_2O as a green and eco-friendly solvent was studied. The reaction conditions were optimized by performing the condensation reaction of benzaldehyde and malononitrile in the presence and absence of the nanocatalyst as well varying the amount of catalyst, temperature and solvent employed in the reaction (Table 1). The use of $Fe_3O_4@SiO_2@CuO–Fe_2O_3$ MNPs was found to be crucial for reaction efficiency. Moreover, the influence of temperature is noteworthy: when the model reaction is performed in H_2O at ambient temperature, low conversion is observed after 40 min. However, running the reaction at reflux dramatically influences the progress of the model reaction after 4 min. Entry 11 shows that conducting the reaction of benzaldehyde (1 mmol) and malononitrile (1.1 mmol) in the presence of $Fe_3O_4@SiO_2@CuO–Fe_2O_3$ MNPs (30 mg) in refluxing H_2O provided satisfactory results.

Next, to pinpoint the main catalytic center of $Fe_3O_4@SiO_2@CuO–Fe_2O_3$, the activity of SiO_2, Fe_3O_4, $Fe_3O_4@SiO_2$, $CuO–Fe_2O_3$ and $SiO_2@CuO–Fe_2O_3$ NPs in the Knoevenagel condensation of benzaldehyde with malononitrile was investigated under the optimized reaction conditions (Table 2). Among the examined NPs, the immobilized $CuO–Fe_2O_3$ on silica-layered magnetite exhibited extraordinary

Table 1 Optimization experiments for the Knoevenagel condensation of benzaldehyde and malononitrile using $Fe_3O_4@SiO_2@CuO–Fe_2O_3$MNPs

Entry	$Fe_3O_4@SiO_2@CuO–Fe_2O_3$ (g)	Solvent	T (°C)	Time (min)	Conversion (%)
1	–	Solvent-free	80	60	Trace
2	–	H_2O	Reflux	60	Trace
3	0.03	Solvent-free	80	40	90
4	0.03	Solvent-free	r.t.	40	60
5	0.03	H_2O	r.t.	40	50
6	0.03	H_2O	70	40	60
7	0.03	$EtOH/H_2O$	70	40	70
8	0.03	EtOH	70	40	20
9	0.03	MeOH	70	40	70
10	0.03	THF	70	40	20
11	0.03	H_2O	Reflux	4	100
12	0.04	H_2O	Reflux	3	100
13	0.02	H_2O	Reflux	15	90

All reactions were carried out with 1 mmol of benzaldehyde and 1.1 mmol of malononitrile in 2 mL of solvent

Table 2 Comparison of the influence of Fe, Si and Cu oxides on the Knoevenagel condensation of benzaldehyde with malononitrile

Entry	Catalyst	Time (min)	Conversion (%)
1	SiO_2	30	45
2	Fe_3O_4	30	80
3	$Fe_3O_4@SiO_2$	30	50
4	$CuO-Fe_2O_3$	15	95
5	$SiO_2@CuO-Fe_2O_3$	15	98
6	$Fe_3O_4@SiO_2@CuO-Fe_2O_3$	4	100

All reactions were carried out with 1 mmol of benzaldehyde, 1.1 mmol of malononitrile and 0.03 g of catalyst in H_2O (2 mL) at reflux

activity in comparison to the singular species, due to the synergistic effect of all compartments (Table 2, entry 6).

The utility of $Fe_3O_4@SiO_2@CuO-Fe_2O_3$ MNPs in the Knoevenagel condensation of structurally diverse aromatic aldehydes with malononitrile was further studied under the optimized reaction conditions. The results of this investigation are summarized in Table 3. All reactions were carried out successfully in refluxing H_2O using the aldehyde (1 mmol), malononitrile (1.1 mmol) and $Fe_3O_4@SiO_2@CuO-Fe_2O_3$ MNPs (30 mg). The corresponding benzylidenemalononitriles were obtained in high to excellent yields within 2–70 min. In the case of terephthalaldehyde and isophthalaldehyde, which possess two formyl groups, the condensation reaction required additional malononitrile (2.2 mmol) and afforded bis-substituted benzylidenemalononitriles in 91–93% yields (Table 3, entries 12 and 13). The calculation shows that 0.03 g of the nanocatalyst contains 0.0171 g CuO (0.00022 mol). Therefore, on the basis of CuO being a main component of the nanocatalyst, TON and TOF values were calculated and the indexed data is presented in Table 3 [84].

The suitability of this synthetic protocol was highlighted by comparison of the Knoevenagel condensation of benzaldehyde and malononitrile with $Fe_3O_4@SiO_2@CuO-Fe_2O_3$ MNPs and other reported reagents (Table 4). The current protocol includes the advantageous in terms of its cost (0.09 USD per 30 mg of the nanocatalyst) and reusability, as well as acceptable yields in shorter reaction times.

A plausible mechanism for the Knoevenagel condensation of aromatic aldehydes and malononitrile catalyzed by $Fe_3O_4@SiO_2@CuO-Fe_2O_3$ MNPs is shown in Scheme 3. Activation of the aromatic aldehyde by the nanocatalyst triggers nucleophilic attack of the methylene group of malononitrile to the activated aldehyde, leading to C–C bond formation. Finally, dehydration of the intermediate gives rise to the benzylidenemalononitrile product.

Recycling of Fe₃O₄@SiO₂@CuO–Fe₂O₃ MNPs

The recoverability of $Fe_3O_4@SiO_2@CuO-Fe_2O_3$ MNPs following the Knoevenagel condensation of benzaldehyde and malononitrile under the optimized reaction

Table 3 The Knoevenagel condensation of aromatic aldehydes and malononitrile by Fe_3O_4@SiO_2@ CuO–Fe_2O_3 MNPs

Entry	Substrate	Product	Time (min)	Yield (%)[a]	TON[b,d]	TOF[c,d]	Mp (°C) Found Reported [Ref]
1	(PhCHO)	(benzylidenemalononitrile)	4	90	4091	61364	81-83 82-84 [64]
2	2-OMe-C6H4CHO	product	15	93	4227	16909	77-79 80 [68]
3	4-MeO-C6H4CHO	product	20	95	4318	12955	113-115 112-114 [67]
4	4-Me-C6H4CHO	product	10	91	4136	24818	137-139 137-138 [68]
5	2-Cl-C6H4CHO	product	5	90	4091	49091	89-91 93-94 [78]
6	4-Cl-C6H4CHO	product	7	91	4136	35455	160-162 161-162 [78]
7	3-O2N-C6H4CHO	product	50	95	4318	5182	102-104 103-105 [78]
8	4-O2N-C6H4CHO	product	40	93	4227	6341	155-157 157-160 [67]
9	2-O2N-4-Cl-C6H3CHO	product	70	96	4364	3740	137-139 –
10	2,4-Cl2-C6H3CHO	product	5	90	4091	49091	141-143 –
11	MeO,HO-C6H3CHO	product	15	97	4409	17636	135-137 134-136 [71]
12	isophthalaldehyde	bis-product	5	93	4227	50727	175-177 –
13	terephthalaldehyde	bis-product	2	91	4136	124091	260-262 295-297 [63]
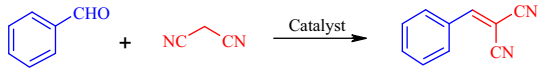
All reactions were carried out with the reaction of aromatic aldehyde (1 mmol), malononitrile (1.1 mmol) and Fe_3O_4@SiO_2@CuO–Fe_2O_3 (30 mg) in refluxing H_2O (2 mL). In entries 12 and 13: malononitrile (2.2 mmol) was used

[a]Yields refer to isolated pure products

[b]TON (turnover number): mmol of product per mmol of catalyst

[c]TOF (turnover frequency): mmol of product per mmol of catalyst per hour

[d]TON and TOF values were calculated on the basis of CuO (30 mg of the nanocatalyst contain 0.00022 mol CuO)

**Table 4** Comparison of the promoter activity of Fe_3O_4@SiO_2@CuO–Fe_2O_3 MNPs with other reported reagents

Entry	Catalyst	Condition/solvent	Time (min)	Yield (%)	Reusability (times)	Refs.
1	Fe_3O_4@SiO_2@CuO–Fe_2O_3 (30 mg)	reflux/H_2O	4	90	5	–
2	Taurine (25 mg)	reflux/H_2O	14	86	6	[63]
3	$PAN_{TT}F$ (81 mg)	20 °C/H_2O	90	99	21	[66]
4	CSC-Star-Glu-IL2 (200 mg)	r.t./H_2O	120	94	5	[67]
5	[C_4dabco][BF_4] (19 mg)	r.t./H_2O	1	100	7	[74]
6	MP(DNP) (14 mg)	r.t./EtOH	3	96	5	[76]
7	ZnO (100 mg)	r.t./solvent-free	80	92	–	[69]
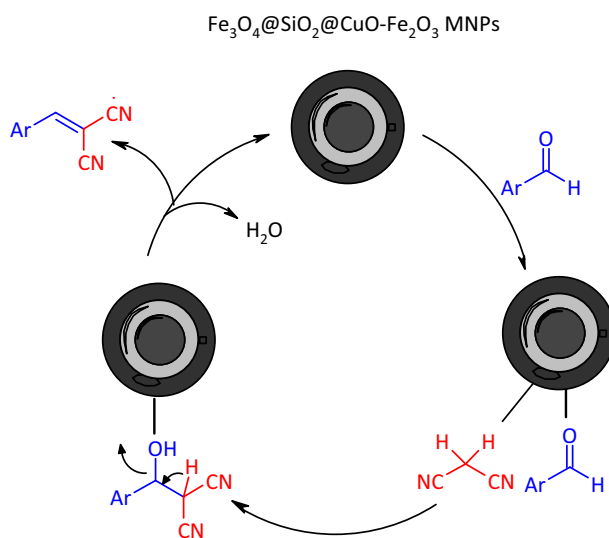
Scheme 3 A plausible mechanism for the Knoevenagel condensation catalyzed by Fe_3O_4@SiO_2@CuO–Fe_2O_3 MNPs

conditions was also studied. After completion of the reaction, the nanocatalyst was separated from the reaction mixture by an external magnetic field, washed with EtOH, and then dried in an oven for subsequent use. The magnetic mixed metal oxide catalyst was able to be reused for five consecutive cycles without significant loss of catalytic activity. The results of this investigation are summarized in Fig. 10.
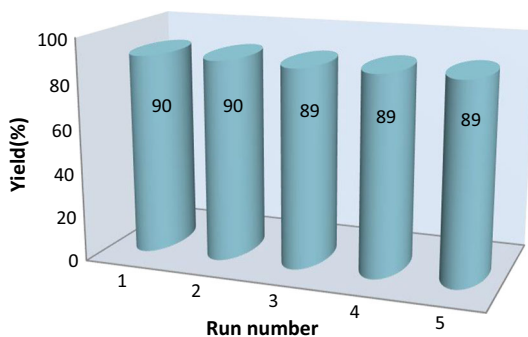
Experimental

General

All chemicals were purchased from Merck Chemical Company and used without further purification. ^1H, ^{13}C NMR and FTIR spectra were recorded on a Bruker Avance spectrometer (300 MHz) and a Thermo Nicolet Nexus 670, respectively. Melting points were obtained in open capillary tubes with a melting point apparatus (Electrothermal) and were uncorrected. Thin-layer chromatography (TLC) on silica gel 60 F_{254} aluminum sheets was used to determine the purity of the substrates and products and to monitor reactions. Powder XRD was obtained by a PANalytical X'Pert Pro (Netherlands) diffractometer at 40 kV and 30 mA with CuKα radiation ($\lambda = 1.5418$ Å), and the diffraction patterns were recorded in the 2θ range (5–80°). The morphology of the nanoparticles was examined by measuring SEM Images using FESEM-TESCAN. The chemical composition of the nanocatalyst was determined by EDX analysis. The N_2 adsorption–desorption isotherms were analyzed on a BELSORP-mini (BET Japan). The specific surface area of the sample was measured by the Brunauer–Emmett–Teller (BET) technique. The pore volume and pore size distribution were derived from the desorption profiles of the isotherms using the Barrett–Joyner–Halenda (BJH) method. The magnetic properties of the samples were obtained using a vibration sample magnetometer VSM (Meghnatis Daghigh Kavir Co., Iran) under magnetic fields of up to 20 kOe. Thermogravimetric analyses (TGA) were recorded on a simultaneous thermal analyzer (STA; Rheometric Scientific Inc.). Transmission electron microscope (TEM) images were obtained using an accelerating voltage of 100 kV on a Zeiss EM10C transmission electron microscope. Inductively coupled plasma optical emission spectrometry (ICP-OES) was utilized for the detection of chemical elements.

Preparation of magnetic Fe_3O_4 NPs

Nanoparticles of Fe_3O_4 were prepared by a chemical co-precipitation of chloride salts of Fe^{2+} and Fe^{3+} [85]. In general, a solution of $FeCl_2 \cdot 4H_2O$ (2.147 g, 0.0108 mol) and $FeCl_3 \cdot 6H_2O$ (5.838 g, 0.0216 mol) in deionized H_2O (100 mL)

was prepared and then the solution was stirred for 10 min at 85 °C under an N_2 atmosphere. Upon addition of ammonia (25 wt%, 10 mL), the black nanoparticles of Fe_3O_4 precipitated. The resulting mixture was again stirred at 85 °C for 30 min under an N_2 atmosphere. The mixture was cooled to room temperature, and the magnetic nanoparticles of Fe_3O_4 were separated by an external magnetic field. Washing the prepared nanoparticles twice with an aqueous solution of NaCl (0.02 M) and deionized H_2O afforded the pure Fe_3O_4 NPs, which were dried under an air atmosphere.

Preparation of $Fe_3O_4@SiO_2$ NPs

Nanoparticles of Fe_3O_4 were coated by a silica layer according to the reported procedure [86]. A suspension of Fe_3O_4 MNPs (1.5 g) in deionized H_2O (20 mL) was prepared. Next, 2-propanol (200 mL) was added and the resulting mixture was irradiated by ultrasound for 30 min. While the mixture was stirred, PEG (5.36 g), deionized H_2O (20 mL), ammonia (28 wt%, 10 ml) and TEOS (2 mL) were added sequentially. The reaction mixture was then stirred for 28 h at room temperature. Finally, the magnetic nanoparticles of $Fe_3O_4@SiO_2$ were separated by an external magnetic field and washed twice with deionized H_2O and EtOH.

Preparation of $Fe_3O_4@SiO_2@CuO–Fe_2O_3$ MNPs

Individually in three beakers (200 mL), a suspension of $Fe_3O_4@SiO_2$ (0.1 g) MNPs in deionized H_2O (50 mL), a solution of Na_2CO_3 (1.589 g, 0.015 mol) and NaOH (0.200 g, 0.005 mol) in deionized H_2O (50 mL), and a solution of $FeCl_3·6H_2O$ (1.352 g, 0.005 mol) and $Cu(NO_3)_2·3H_2O$ (3.624 g, 0.015 mol) in deionized H_2O (50 mL) was prepared. The resulting suspension and solutions were irradiated under ultrasound for 30 min. The prepared solutions of $FeCl_3·6H_2O/Cu(NO_3)_2·3H_2O$ and $Na_2CO_3/NaOH$ were then simultaneously added dropwise to the suspension of $Fe_3O_4@SiO_2$, and the resulting mixture was stirred vigorously. During the course of the reaction, the pH was kept at 10–11 by the addition of an appropriate volume of aqueous NaOH and HCl. The resulting slurry was left for 24 h at 80 °C without stirring. The resulting mixture was cooled to room temperature and washed with deionized H_2O and EtOH. Calcination at 150 °C for 2 h afforded magnetic nanoparticles of $Fe_3O_4@SiO_2@CuO–Fe_2O_3$ (total weight: 2.091 g; $Fe_3O_4@SiO_2$: 0.1 g, 4.78%; CuO: 1.193 g, 57.05% and Fe_2O_3: 0.798 g, 38.16%).

General procedure for the Knoevenagel condensation of benzaldehyde and malononitrile

In a round-bottom flask (10 mL) equipped with a magnetic stirrer, a mixture of benzaldehyde (0.106 g, 1 mmol), malononitrile (0.073 g, 1.1 mmol) and H_2O (2 mL) was well mixed at room temperature. $Fe_3O_4@SiO_2@CuO–Fe_2O_3$ (30 mg) was then added and the resulting mixture was stirred for 4 min at reflux. The progress of the reaction was monitored by TLC (eluent: EtOAc/*n*-hexane: 2/4). After completion of the reaction, the catalyst was separated by an external magnet

and the reaction mixture was extracted with EtOAc (2×5 mL). The organic solution was then dried over anhydrous Na_2SO_4. Evaporation of the solvent afforded the pure benzylidenemalononitrile in 90% yield (0.139 g, Table 3, entry 1).

Conclusions

In this study, magnetic nanoparticles of immobilized $CuO–Fe_2O_3$ on silica-layered magnetite were synthesized. The magnetite mixed metal oxide was then characterized using FTIR, SEM, EDX, XRD, BET, TGA, DTG, VSM, TEM and ICP-OES analyses. The prepared $Fe_3O_4@SiO_2@CuO–Fe_2O_3$ MNPs were successfully utilized in the Knoevenagel condensation of structurally diverse aromatic aldehydes and malononitrile in refluxing H_2O. The corresponding benzylidenemalononitriles were obtained in high to excellent yields within 2–70 min. This method has several advantages, including high yields, short reaction times, mild reaction conditions, a simple separation and work-up procedure, and the use of H_2O as a green and economical solvent. The catalyst can be reused for at least five consecutive cycles without significant loss of catalytic activity.

References

1. B. Aday, Y. Yildiz, R. Ulus, S. Eris, F. Sen, M. Kaya, New J. Chem. **40**, 748 (2016)
2. H. Goksu, Y. Yildiz, B. Celik, M. Yazici, B. Kilbas, F. Sen, Catal. Sci. Technol. **6**, 2318 (2016)
3. F. Sen, G. Gokagac, S. Sen, J. Nanopart. Res. **15**, 1979 (2013)
4. B. Aday, H. Pamuk, M. Kaya, F. Sen, J. Nanosci. Nanotechnol. **16**, 6498 (2016)
5. Y. Yildiz, E. Erken, H. Pamuk, H. Sert, F. Sen, J. Nanosci. Nanotechnol. **16**, 5951 (2016)
6. O. Karatepe, Y. Yildiz, H. Pamuk, S. Eris, Z. Dasdelen, F. Sen, RSC Adv. **6**, 50851 (2016)
7. Y. Yildiz, S. Kuzu, B. Sen, A. Savk, S. Akocak, F. Sen, Int. J. Hydrogen Energy **42**, 13061 (2017)
8. E. Erken, Y. Yildiz, B. Kilbas, F. Sen, J. Nanosci. Nanotechnol. **16**, 5944 (2016)
9. Y. Yildiz, T. Onal Okyay, B. Sen, B. Gezer, S. Kuzu, A. Savk, E. Demir, Z. Dasdelen, H. Sert, F. Sen, ChemistrySelect **2**, 697 (2017)
10. S. Akocak, B. Sen, N. Lolak, A. Savk, M. Koca, S. Kuzu, F. Sen, Nano Struct. Nano Objects **11**, 25 (2017)
11. H. Goksu, B. Celik, Y. Yildiz, F. Sen, B. Kilbas, ChemistrySelect **1**, 2366 (2016)
12. B. Sen, S. Kuzu, E. Demir, T.O. Okyay, F. Sen, Int. J. Hydrogen Energy **42**, 23299 (2017)
13. Z. Dasdelen, Y. Yildiz, S. Eris, F. Sen, Appl. Catal. B Environ. **219**, 511 (2017)
14. B. Sena, E. Hazal Akdere, A. Savk, E. Gultekin, O. Parali, H. Goksu, F. Sen, Appl. Catal. B Environ. **225**, 148 (2018)
15. I. Esirden, E. Erken, M. Kaya, F. Sen, Catal. Sci. Technol. **5**, 4452 (2015)
16. B. Celik, Y. Yildiz, H. Sert, E. Erken, Y. Koskun, F. Sen, RSC Adv. **6**, 24097 (2016)
17. B. Celik, E. Erken, S. Eris, Y. Yildiz, B. Sahin, H. Pamuk, F. Sen, Catal. Sci. Technol. **6**, 1685 (2016)
18. E. Erken, I. Esirden, M. Kaya, F. Sen, RSC Adv. **5**, 68558 (2015)
19. Y. Yildiz, H. Pamuk, O. Karatepe, Z. Dasdelen, F. Sen, RSC Adv. **6**, 32858 (2016)
20. H. Goksu, Y. Yildiz, B. Celik, M. Yazici, B. Kilbas, F. Sen, ChemistrySelect **1**, 953 (2016)
21. M. Gilanizadeh, B. Zeynizadeh, New J. Chem. (2018). https://doi.org/10.1039/C8NJ00788H
22. S.U. Sonavane, M.B. Gawande, S.S. Deshpande, A. Venkataraman, R.V. Jayaram, Catal. Commun. **8**, 1803 (2007)

23. Y. Izumi, N. Natsume, H. Takamine, I. Tamaoki, K. Urabe, Bull. Chem. Soc. Jpn. **62**, 2159 (1989)
24. K. Tanabe, W.F. Holderich, Appl. Catal. A **181**, 399 (1999)
25. B.M. Reddy, A. Khan, Catal. Rev. Sci. Eng. **47**, 257 (2005)
26. S. Ajaikumar, A. Pandurangan, Appl. Catal. A **357**, 184 (2009)
27. W.C. Sheets, E.S. Stampler, H. Kabbour, M.I. Bertoni, L. Cario, T.O. Mason, T.J. Marks, K.R. Poeppelmeier, Inorg. Chem. **46**, 10741 (2007)
28. A. Tang, H. Yang, X. Zhang, Int. J. Phys. Sci. **1**, 102 (2006)
29. V.V. Zyryanov, Inorg. Mater. **39**, 1163 (2003)
30. H. Cui, M. Zayat, D. Levy, J. Sol-Gel Sci. Technol. **35**, 175 (2005)
31. A. Elia, P.M. Aispuro, N. Quaranta, J.M. Martın-Martınez, P. Vazquez, Macromol. Symp. **301**, 136 (2011)
32. Y.J. Kim, S.B. Rawal, S.D. Sung, W.I. Lee, Bull. Korean Chem. Soc. **32**, 141 (2011)
33. P.F. Fulvio, S. Pikus, M. Jaroniec, A.C.S. Appl. Mater. Interfaces **2**, 134 (2010)
34. D. Jiang, L. Su, L. Ma, N. Yao, X. Xu, H. Tang, X. Li, Appl. Surf. Sci. **256**, 3216 (2010)
35. B.M. Reddy, I. Ganesh, J. Mol. Catal. A Chem. **169**, 207 (2001)
36. B.M. Reddy, B. Chowdhury, P.G. Smirniotis, Appl. Catal. A **211**, 19 (2001)
37. G. Sankar, C.N.R. Rao, T. Rayment, J. Mater. Chem. **1**, 299 (1991)
38. A.S. Kulkarni, R.V. Jayaram, J. Mol. Catal. A Chem. **223**, 107 (2004)
39. Y.C. Chang, S.W. Chang, D.H. Chen, React. Funct. Polym. **66**, 335 (2006)
40. V. Polshettiwar, R. Luque, A. Fihri, H. Zhu, M. Bouhrara, J.M. Basset, Chem. Rev. **111**, 3036 (2011)
41. R. Abu-Reziq, H. Alper, D. Wang, M.L. Post, J. Am. Chem. Soc. **128**, 5279 (2006)
42. M. Shokouhimehr, Y. Piao, J. Kim, Y. Jang, T. Hyeon, Angew. Chem. Int. Ed. **46**, 7039 (2007)
43. D.H. Zhang, G.D. Li, J.X. Li, J.S. Chen, Chem. Commun. 3414 (2008)
44. A.H. Lu, E.L. Salabas, F. Schuth, Angew. Chem. Int. Ed. **46**, 1222 (2007)
45. M.B. Gawande, P.S. Branco, R.S. Varma, Chem. Soc. Rev. **42**, 3371 (2013)
46. S. Shylesh, V. Schünemann, W.R. Thiel, Angew. Chem. Int. Ed. **49**, 3428 (2010)
47. S.M. Baghbanian, M. Farhang, Synth. Commun. **44**, 697 (2014)
48. A.P. Amrute, A. Bordoloi, N. Lucas, K. Palraj, S.B. Halligudi, Catal. Lett. **126**, 286 (2008)
49. S.J. Singh, R.V. Jayaram, Tetrahedron Lett. **49**, 4249 (2008)
50. Q. Shi, R. Lu, L. Lu, X. Fu, D. Zhao, Adv. Synth. Catal. **349**, 1877 (2007)
51. M. Kang, E.D. Park, J.M. Kim, J.E. Yie, Catal. Today **111**, 236 (2006)
52. N. Li, C. Descorme, M. Besson, Appl. Catal. B **76**, 92 (2007)
53. S.S. Deshpande, R.V. Jayaram, Catal. Commun. **9**, 186 (2008)
54. Q. Zhuang, J.M. Miller, Appl. Catal. A **209**, L1 (2001)
55. M. Crivello, C. Pe´rez, E. Herrero, G. Ghione, S. Casuscelli, E. Rodrıguez-Castellon, Catal. Today **107–108**, 215 (2005)
56. A.K. Singh, S.D. Fernando, Energy Fuels **23**, 5160 (2009)
57. G. Centi, S. Perathoner, Catal. Rev. Sci. Eng. **40**, 175 (1998)
58. M.A. Carreon, V.V. Guliants, Eur. J. Inorg. Chem. **2005**, 27 (2005)
59. L.F. Tietze, U. Beifuss, *Comprehensive Organic Synthesis*, vol. 2 (Pergamon Press, Oxford, 1991), p. 341
60. F. Freeman, Chem. Rev. **69**, 591 (1969)
61. R.K.G. Panicker, S. Krishnapillai, Tetrahedron Lett. **55**, 2352 (2014)
62. M. Almasi, V. Zelenak, M. Opanasenko, J. Cejka, Dalton Trans. **43**, 3730 (2014)
63. F. Shirini, N. Daneshvar, RSC Adv. **6**, 110190 (2016)
64. S. Wang, Z. Ren, W. Cao, W. Tong, Synth. Commun. **31**, 673 (2001)
65. J. Zhang, T. Jiang, B. Han, A. Zhu, X. Ma, Synth. Commun. **36**, 3305 (2006)
66. G. Li, J. Xiao, W. Zhang, Green Chem. **14**, 2234 (2012)
67. P. Gupta, M. Kour, S. Paul, J.H. Clark, RSC Adv. **4**, 7461 (2014)
68. M.M. Heravi, K. Bakhtiari, S. Taheri, H.A. Oskooi, J. Chin. Chem. Soc. **54**, 1557 (2007)
69. M. Basude, P. Sunkara, V.S. Puppala, J. Chem. Pharm. Res. **5**, 46 (2013)
70. M.A. Pasha, K. Manjula, V.P. Jayashankara, Indian J. Chem. **49**, 1428 (2010)
71. R. Pal, Int. J. Adv. Chem. **2**, 27 (2014)
72. R. Gupta, M. Gupta, S. Paul, R. Gupta, Bull. Korean Chem. Soc. **30**, 2419 (2009)
73. W.X. Zuo, R. Hua, X. Qiu, Synth. Commun. **34**, 3219 (2004)
74. D.Z. Xu, Y. Liu, S. Shi, Y. Wang, Green Chem. **12**, 514 (2010)
75. A. Rostami, B. Atashkar, H. Gholami, Catal. Commun. **37**, 69 (2013)
76. S.K. Panja, N. Dwivedi, S. Saha, RSC Adv. **5**, 65526 (2015)

77. R. Vaid, M. Gupta, Monatshefte Chem. **146**, 645 (2015)
78. S.L. Khillare, A.O. Dhokte, M.K. Lande, B.R. Arbad, Int. J. Chem. Pharm. Sci. **5**, 96 (2014)
79. M. Gupta, R. Gupta, M. Anand, Beilstein J. Org. Chem. **5**, 68 (2009)
80. C. Zhuo, D. Xian, W. Jian-wei, X. Hui, ISRN Org. Chem. 676789 (2011)
81. G.Y. Li, Y.R. Jiang, K.L. Huang, P. Ding, L.L. Yao, Colloids Surf. A Physicochem. Eng. Asp. **320**, 11 (2008)
82. J.A. Lopez, F. González, F.A. Bonilla, G. Zambrano, M.E. Gómez, Rev. LatinAm. Metal. Mater. **30**, 60 (2010)
83. A. Azam, A.S. Ahmed, M. Oves, M.S. Khan, S.S. Habib, A. Memic, Int. J. Nanomed. **7**, 6003 (2012)
84. J.J. Boruah, S.P. Das, S.R. Ankireddy, S.R. Gogoi, N.S. Islam, Green Chem. **15**, 2944 (2013)
85. X. Liu, Z. Ma, J. Xing, H. Liu, J. Magn. Magn. Mater. **270**, 1 (2004)
86. Y. Zhang, G.M. Zeng, L. Tang, D.L. Huang, X.Y. Jiang, Y.N. Chen, Biosens. Bioelectron. **22**, 2121 (2007)